

Simulation and Analysis of Molecular Bottlebrush Dynamics in Dilute Solutions

Raj S. Mukkamala and Michael J. A. Hore*

Cite This: *Macromolecules* 2024, 57, 445–455

Read Online

ACCESS |



Metrics & More

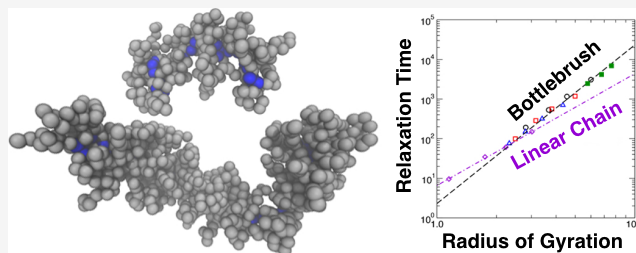


Article Recommendations



Supporting Information

ABSTRACT: Molecular bottlebrushes consist of a linear polymer backbone that is densely grafted with side chains. They have received considerable attention due to their unique physical properties (e.g., very high entanglement molecular weights) relative to linear homopolymers. To date, their relaxation dynamics have received significantly less attention than their conformation and self-assembly. In this article, we make use of dissipative particle dynamics (DPD) simulations with proper orthogonal decomposition (POD) to study the relaxation dynamics of bottlebrushes in dilute solutions. The modes obtained by POD suggest that the backbone behaves identically to a linear chain and that the motions of its monomers are coupled to the side chains because of their grafted state. Although simulations of linear chains behaved as expected from the Zimm model, the scaling of the relaxation times of the bottlebrushes with R_g followed an unexpected scaling relationship $\tau \sim R_g^{3.4}$. Our simulations demonstrate that the origin of this scaling law resides in differences between the scaling of R_g and the hydrodynamic radius R_h as the bottlebrush molecular weight is varied and that the Zimm model accurately describes dilute solutions of bottlebrushes.



INTRODUCTION

Molecular bottlebrushes form from a dense grafting of side chains to a macromolecular backbone and can be synthesized in several ways.¹ First, atom-transfer radical polymerization (ATRP) can be used to first polymerize a linear backbone, after which additional initiation sites can be installed along the backbone so that side chains can be “grafted from” the backbone to form the bottlebrush. Another common method that uses ring opening metathesis polymerization (ROMP) has become a popular means for synthesizing bottlebrushes from norbornyl-functionalized macromonomers. Such macromonomers can be synthesized by traditional controlled radical polymerization techniques (e.g., RAFT or ATRP).² This “graft-through” method offers a vast number of accessible side chain chemistries while also allowing for multiple side chains per backbone site.³ Combining ROMP with recent advances in synthesis has produced families of precise bottlebrushes with discrete side chains ($D = 1.0$) and a number of different topologies.⁴ Finally, bottlebrushes can be synthesized with a “grafting-to” approach by grafting side chains to a pre-existing polymer backbone.⁵

Bottlebrushes, or polymacromonomers as they have also been referred to historically,^{6–11} have received considerable attention in recent years due to unique physical properties that result from their architecture.¹² For example, bottlebrushes possess very large entanglement molecular weights (M_e) compared to those of traditional linear polymers. For typically accessible bottlebrush molecular weights, $M_n < M_e$ meaning that they effectively do not experience entanglements. Cai et

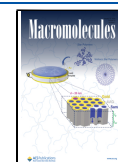
al.¹³ took advantage of the lack of entanglements to synthesize ultrasoft polymer gels which might be used in biomedical applications. Other work has investigated the potential of bottlebrush-like molecules for single-molecule electronics,^{14,15} artificial mucins,¹⁶ and modulating their biological function^{17,18} among many other applications.^{1,19–22} In all of these examples, the conformation of the bottlebrush, whether in terms of the backbone, side chains, or entire molecule, was central to the properties of the materials that they comprised. For instance, Kruger et al.¹⁶ synthesized two chemically identical bottlebrushes using either Schrock’s tungsten alkylidene catalyst, which produced *cis*-rich bottlebrushes, or Grubbs’ ruthenium catalyst, which produced *trans*-rich bottlebrushes. The choice of the catalyst ultimately affected the shape of the bottlebrushes, with *cis*-rich bottlebrushes exhibiting worm-like conformations and *trans*-rich bottlebrushes forming globules, as observed with atomic force microscopy (AFM) and small-angle neutron scattering (SANS) measurements. While the worm-like bottlebrushes resembled natural mucins and functioned as such, globular bottlebrushes did not express any useful biological function.

Received: November 4, 2023

Revised: December 20, 2023

Accepted: December 26, 2023

Published: January 9, 2024



The assembly and conformation of bottlebrushes have been previously studied by multiple techniques, including Monte Carlo simulations,^{23,24} polymer field theory,^{3,25,26} molecular/Brownian dynamics simulations,^{24,27–34} PRISM,³⁰ analytical theories/scaling analysis,^{29,32} light/neutron scattering,^{6,7,9,10,14,16–18,35–37} and many others. Taken together, this body of work is generally in agreement with regard to the shape of bottlebrushes, and here, we briefly highlight only some select results from prior simulations. Given the large parameter space available for bottlebrushes, early Monte Carlo simulations focused on experimentally relevant values of backbone (N_{bb}) and side chain (N_{sc}) lengths and found that the backbone radius of gyration scaled as $R_{g,bb} \sim N_{bb}^{0.62}$, while the side chains obeyed a stronger scaling $R_{g,sc} \sim N_{sc}^{0.68}$.²³ These scaling relations arise because for typical bottlebrush molecular weights, the molecules exist in an intermediate regime between rod-like conformations for short backbones and those described by random walks which are expected to arise for very high molecular weights. For this reason, Binder and co-workers²⁴ proposed that many mass scaling relationships (e.g., for R_g with N) obtained for bottlebrushes may not be particularly relevant. Nevertheless, these relationships may be useful in the interpretation of small-angle scattering measurements. In their Monte Carlo simulations, Binder et al. extensively explored the conformation of bottlebrushes at several length scales and quantitatively matched experimental SANS measurements.²⁴ More recent calculations of the overall bottlebrush shape from the gyration tensor³⁷ found that bottlebrushes were roughly spherical for short backbone lengths and became increasingly anisotropic as the backbone length increased. These observations were in general agreement with complementary SANS measurements. Grubbs and co-workers have shown that in solution, bottlebrush concentration³⁸ can affect conformational properties such as the anisotropy of the molecule, and care must be taken when choosing models to fit small-angle scattering measurements since strong correlations between structural parameters can be present.³⁹

To date, investigations into the relaxation dynamics of bottlebrushes are more scarce in the literature than structural studies. Rheological measurements of polyolefin bottlebrush melts have shown that relaxations at short times followed predictions from the Zimm model, but as the length scale increased Rouse-like relaxations emerged.⁴⁰ Importantly, the Zimm-like dynamics were not attributed to hydrodynamic interactions but rather to shielding effects near the backbone that mimicked the hydrodynamics in the solution state. At longer times, the bottlebrushes behaved as though they were unentangled Gaussian chains. These observations are also supported by dynamic light scattering (DLS) measurements⁴¹ that suggest similar relaxation modes for linear polymers and bottlebrushes so long as their contours (e.g., the backbone of the bottlebrush) are similar. Other DLS measurements that compared polyelectrolyte bottlebrushes to analogous linear polymers observed that although the behaviors of the two architectures were similar, the relaxation times of the bottlebrushes were at least a factor of 2 longer than for the linear chains.⁴² Broadband dielectric spectroscopy (BDS) measurements of poly(dimethylsiloxane)-based (PDMS) bottlebrushes primarily observed segmental relaxations of the side chains due to the much larger number of dipoles present in those portions of the molecule. Compared to free side chains, the grafted side chains exhibited dynamics that were roughly

an order of magnitude slower for the lowest molecular weight chains, although this effect became less pronounced as the side chain length increased and confinement was reduced. Bichler et al.⁴³ compared the dynamics of solid-state PDMS linear polymers to bottlebrushes and found that architectural differences between the two classes of molecules did not impact segmental dynamics beyond an increase in the relaxation time for the bottlebrush system, in general agreement with the solution-state measurements by Horkay et al.⁴² Prior to diffusive motions of the bottlebrushes or entanglements of the linear polymers, the dynamics of both architectures followed the Rouse description. Quasi-elastic neutron scattering (QENS) measurements using neutron backscattering were largely in agreement with these BDS measurements.⁴⁴ More recent QENS measurements⁴⁵ using neutron spin-echo spectroscopy focused on PDMS bottlebrushes with either short or long side chains. QENS measurements of the samples with shorter side chains were thought to be more sensitive to backbone dynamics, whereas the longer side chain samples were more representative of the dynamics of the entire bottlebrush. For values of the scattering vector Q that matched the length scales of interest of the molecule, the authors found that the relaxation times of the backbone and entire molecule were scaled as $\tau \sim Q^{-2.5}$ and $\tau \sim Q^{-3.9}$, respectively. To the best of our knowledge, no extensive simulation studies of the relaxation dynamics of molecular bottlebrushes exist in the literature. Such simulations are made difficult by the fact that Rouse mode analysis may not be applicable to the bottlebrush architecture without first identifying an appropriate basis for calculating the normal coordinates.

Motivated by these previous studies, we show in this article that proper orthogonal decomposition (POD) can be used to study the dynamics of both the backbone and the entirety of a bottlebrush molecule. In this study, we used dissipative particle dynamics (DPD) simulations, coupled with POD, to study and analyze the dynamics of bottlebrush polymers in dilute, good solvent conditions. First, we verified that DPD and our parameter set produced bottlebrushes and observed how varying the backbone length and side chain spacing affected the conformation of the molecules. Next, we calculated the modes for a bottlebrush and used them to perform mode analysis in our simulations to understand the dynamics of the bottlebrushes. Finally, we investigated the scaling of the longest relaxation time of the bottlebrush and its backbone as a function of the architectural parameters (e.g., backbone length) and compared the results to prior experimental investigations by others. The results of this study are in good agreement with previous experimental results and help to coalesce our understanding of their dynamics while also suggesting new avenues that may be explored in the future to better understand this class of polymers.

MODEL AND METHODS

Dissipative Particle Dynamics (DPD). The temporal evolution of dilute bottlebrush solutions was simulated using DPD. DPD is a coarse-grained particle dynamics technique that preserves hydrodynamic interactions and can access mesoscopic time scales due to the use of a soft-repulsive conservative force. Forces act between particles within a cutoff distance r_c , and r_c is used to define the fundamental unit of length in DPD. We focused exclusively on good solvent conditions, while systematically varying the backbone length (N_{bb}) and the number of monomers along the backbone between side chain grafting points (N_x). Each bottlebrush was grafted with $n_s =$

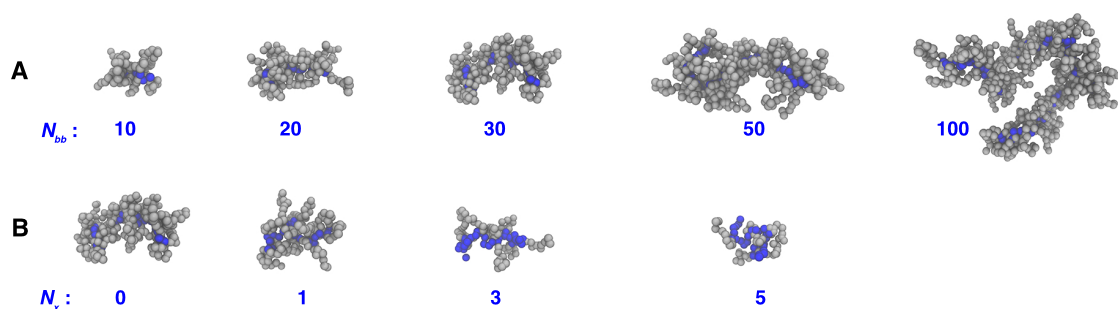


Figure 1. Simulation snapshots showing the effect of architectural parameters on the bottlebrush structure. (A) Effect of increasing backbone length (N_{bb}) for $N_{sc} = 10$ and $N_x = 0$. (B) Effect of increasing side chain spacing (N_x) for $N_{bb} = 30$ and $N_{sc} = 10$.

$N_{bb}/(N_x + 1)$ side chains and had a total degree of polymerization of $N_{tot} = N_{bb} + n_s N_{sc}$. Simulations were performed at a particle density of $\rho = 3 r_c^{-3}$ in a cubic system with periodic boundary conditions and a lateral size of $L_x = L_y = L_z = 48 r_c$. The system size was chosen to be much larger (8–10 \times) than the largest value of the radius of gyration (R_g) of a bottlebrush to minimize the effects of any potential interchain interactions. In all simulations, the bottlebrush volume fraction was fixed at $\phi_p = 0.05$, with the number of polymers in the simulation box given by $n_p = \phi_p \rho L_x L_y L_z / N_{tot}$. In practice, n_p varied between approximately 50 and 500 polymers depending on the value of N_{tot} . As illustrated in the Supporting Information (Figure S1), for $\phi_p \leq 0.1$, we observed no effect of polymer volume fraction on our results. We used our in-house parallel DPD code (PD²) for all simulations.

In DPD, coarse-grained fluid elements (“DPD beads”) separated by distances less than r_c interact through a conservative, random, and dissipative force. The soft-repulsive conservative force in essence assigns a particle type to the DPD beads through interaction strength a_{ij} while the random and dissipative forces combine to form the thermostat for the simulation. These forces are pairwise between particles i and j and read

$$\begin{aligned} \mathbf{F}_{ij}^C &= a_{ij} w^R(r_{ij}) \hat{\mathbf{r}}_{ij} \\ \mathbf{F}_{ij}^R &= \sigma (\Delta t)^{-1/2} w^R(r_{ij}) \theta_{ij} \hat{\mathbf{r}}_{ij} \\ \mathbf{F}_{ij}^D &= -\gamma w^D(r_{ij}) (\hat{\mathbf{r}}_{ij} \cdot \mathbf{v}_{ij}) \hat{\mathbf{r}}_{ij} \end{aligned} \quad (1)$$

where $\mathbf{r}_{ij} = \mathbf{r}_i - \mathbf{r}_j$, $r_{ij} = |\mathbf{r}_{ij}|$, $\hat{\mathbf{r}}_{ij} = \mathbf{r}_{ij}/r_{ij}$ and $\mathbf{v}_{ij} = \mathbf{v}_i - \mathbf{v}_j$. In addition to the three DPD forces, bonded monomers were connected by a FENE potential using identical parameters to our previous work.⁴⁶ θ_{ij} is a symmetric random variable with $\langle \theta_{ij} \rangle = 0$ and $\langle \theta_{ij}^2 \rangle = 1$, which is unique for each pair of particles at each time step. The fluctuation–dissipation theorem requires that the coefficients of the random and dissipative forces be related to each other by $\sigma^2 = 2\gamma k_B T$, in which we set $\epsilon_0 = k_B T = 1$. Although not required, the weight factors for the dissipative and conservative forces are commonly related by $w^D(r_{ij}) = [w^R(r_{ij})]^2$, where

$$w^R(r_{ij}) = \begin{cases} 1 - \frac{r_{ij}}{r_c}, & r_{ij} < r_c \\ 0, & r_{ij} \geq r_c \end{cases} \quad (2)$$

with the cutoff distance $r_c = 1$. The interaction strengths between all particles were fixed at $a_{ij} = 25\epsilon_0/r_c$ which has been previously shown to produce good solvent conditions for DPD simulations of polymer solutions.^{47,48}

Finally, the DPD bead positions and velocities were updated from time $t \rightarrow t + \Delta t$ by integrating Newton’s second law using the velocity-Verlet algorithm with a time step of $\Delta t = 0.01 \tau_0$.⁴⁹ Simulations were performed by initializing bottlebrushes and their monomers at random positions in the simulation box and allowing them to equilibrate such that $k_B T \approx 1$ and R_g saturated to a constant value, which occurred within 10^5 time steps. After equilibration, we performed 3×10^6 production time steps over which we collected

monomer information for analyzing the relaxation dynamics. For the largest bottlebrushes, it was occasionally necessary to run the simulations for longer times ($\approx 8 \times 10^6$ time steps) to ensure that $C_p(t)$, described below, decayed to below 0.1.

Proper Orthogonal Decomposition (POD). The time scales of bottlebrush relaxations were studied using POD, which is an approach closely related to principal component analysis (PCA) and singular value decomposition (SVD). In traditional simulations of linear homopolymers, Rouse mode analysis is used to observe the time necessary for the normal coordinates $\mathbf{X}_p(t)$ of the polymers to become uncorrelated in time, where p is the mode number. The normal coordinate is related to the amplitude of each mode.⁵⁰ For such polymers, the normal coordinates are given by cosine transforms of the monomer positions $\mathbf{r}_i(t)$

$$\mathbf{X}_p(t) = \sqrt{\frac{2}{N}} \sum_{i=1}^N \cos\left[\frac{p\pi}{N}\left(i - \frac{1}{2}\right)\right] \mathbf{r}_i(t) \quad (3)$$

The relaxation time for each p is computed from the autocorrelation function of $\mathbf{X}_p(t)$

$$C_p(t) = \frac{\langle \mathbf{X}_p(t) \mathbf{X}_p(0) \rangle}{\langle \mathbf{X}_p^2 \rangle} \sim \exp\left[-\left(\frac{t}{\tau_p}\right)^{\beta_p}\right] \quad (4)$$

where $0 \leq \beta_p \leq 1$ is a stretching exponent and τ_p is the relaxation time of mode p . As β_p decreases, the relaxation dynamics become increasingly heterogeneous. Previous studies using POD, which is described in detail below, have obtained best fits to $C_p(t)$ using $\beta_p = 1$, which we will also use throughout the remainder of this paper.^{46,51}

Strictly speaking, the cosine basis appearing in eq 3 is valid only for linear homopolymers. Similar relationships can be derived for other polymer architectures, such as statistical copolymers⁵² and star polymers,⁵³ but in practice it may be challenging to analytically identify the correct eigenvectors for a given polymer architecture. For this reason, in the present study, $C_p(t)$ was calculated using normal coordinates that were obtained numerically by POD. In this approach, snapshots of the monomer positions for each bottlebrush are stored to construct a covariance matrix \mathbf{M} for each $q = x, y, \text{ or } z$ coordinate of the monomers, where

$$M_{ij}^q = \frac{1}{T} \sum_{t=0}^{T-1} q_i'(t) q_j'(t) \quad (5)$$

In the above expression, T is the total number of snapshots of the coordinates and $q_i'(t)$ denotes, at time t , the distance between particle i and the center of mass of the molecule it comprises.^{46,51} The $x, y,$ and z components are treated independently, and the results are averaged to reduce statistical fluctuations in the results.

The normalized eigenvectors ψ_p of \mathbf{M} , when ordered by decreasing value of their corresponding eigenvalue, represent the basis necessary to obtain $\mathbf{X}_p(t)$ from $\mathbf{r}_i(t)$ for the $p = 1, 2, \dots, N$ th mode, as in eq 3. In other words, when using POD, the normal coordinates for a given bottlebrush are computed as the product

$$\mathbf{X}_p(t) = \psi_p^n \times [\mathbf{x}_n(t)\mathbf{y}_n(t)\mathbf{z}_n(t)] \quad (6)$$

where the vector $\mathbf{x}_n(t)$ contains the x -coordinates of the $n = 1, 2, \dots, N$ monomers in the bottlebrush as components, and so on. The normal coordinate autocorrelation $C_p(t)$ is then computed by using eq 4.

RESULTS AND DISCUSSION

Bottlebrush Structure. Polymer conformation influences the relaxation dynamics. For example, the dynamics of unentangled polymers in the absence of hydrodynamic effects can be described by the Rouse model, where the relaxation time of mode p scales as $\tau_p \sim (N/p)^{(2\nu+1)} \sim R_g^{(2\nu+1)/\nu}$. Information about the chain conformation is contained in Flory parameter ν , which describes the scaling of R_g with N . When hydrodynamics play an important role, the Zimm model predicts $\tau_p \sim (N/p)^{3\nu} \sim R_g^3$. Although the scaling of τ_p with R_g is sensitive to polymer conformation in the Rouse model, the scaling of τ_p with R_g is independent of ν in the Zimm model.

Because of the relationship between polymer conformation and dynamics, we evaluated how varying the key architectural parameters of the bottlebrushes influenced their size and shape since our DPD simulations use different parameters than previous molecular dynamics or Monte Carlo simulations. Snapshots of representative bottlebrushes are shown in Figure 1a for different values of the backbone length (N_{bb}) at fixed values of $N_{sc} = 10$ and $N_x = 0$. Backbone and side chain monomers are rendered as blue and gray beads, respectively. Qualitatively we observe that as N_{bb} increases from 10 to 100 (left to right), the molecule becomes increasingly anisotropic and worm-like in its shape. This behavior has been observed in several prior simulation studies by others.^{27,31,32,37} Figure 1b highlights the effect of increasing N_x (left to right) for fixed values of $N_{bb} = 30$ and $N_{sc} = 10$, with both the entire molecule and backbone becoming less elongated as N_x increases.

In Figure 2a, we plot the radius of gyration of the backbone ($R_{g,bb}$) as a function of its length on a double logarithmic scale for $N_x = 0-5$ and $N_{sc} = 10$. The backbone is elongated for $N_x = 0$, with $R_g \sim (N_{bb} - 1)^{0.73}$, which is similar to the scaling exponent of $\nu \approx 0.7$ observed by both Yethiraj²³ and Dutta et al.,³⁷ but slightly larger than the exponent of 0.62 observed by Binder et al.²⁴ This indicates that for the set of parameters considered here, the bottlebrushes are within the transition region between highly elongated conformations and more ideal conformations that are expected to arise for sufficiently long backbones. In addition, we observe that the scaling exponent decreases as N_x increases due to reduced crowding by the side chains, which allows the backbone to adopt a more ideal conformation. Despite the relatively elongated conformation of the backbone, we observe a weaker scaling of $R_{g,tot}$ with N_{bb} . In Figure 2b, we plot $R_{g,tot}$ as a function of the total degree of polymerization N_{tot} on a double logarithmic scale and observe a few behaviors. First, $R_{g,tot}$ decreases as N_x increases, as expected from the snapshots shown in Figure 1b. Second, the scaling of R_g with N_{tot} becomes weaker as N_x increases, decreasing from $\nu \approx 0.56$ ($N_x = 0$) to $\nu \approx 0.50$ ($N_x = 5$). These scaling exponents are similar to those measured experimentally using SANS.^{14,16,17,35}

Finally, the hydrodynamic radius of bottlebrush R_h is shown in Figure 3a. Although the radius of gyration of the molecules obeys different scaling laws for different values of N_x , we observe that R_h follows a single power law for all values of N_x , implying that the ratio R_g/R_h varies as N_{tot} increases and as N_x is changed. Previous work by others^{31,37} has observed that this

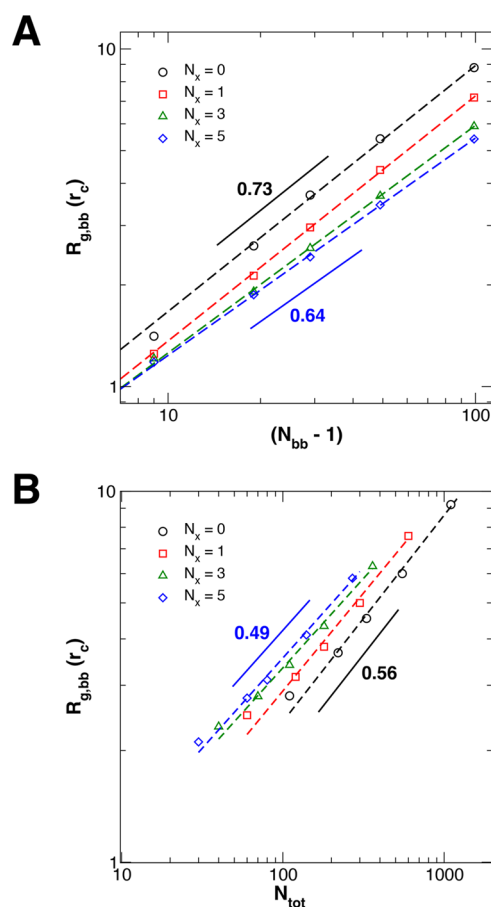


Figure 2. Variation of the bottlebrush size as a function of architectural parameters. (A) R_g of the backbone as a function of its length for different values of N_x and (B) R_g for the entire molecule as a function of its total degree of polymerization for different values of N_x . For all data, error bars are smaller than the size of the points.

ratio is not constant for bottlebrushes and exhibits a minimum for intermediate values of N_{tot} . We plot this ratio in Figure 3b for both the bottlebrushes (open points) and linear polymers (solid triangles) as a function of the radius of gyration of the molecules. For the linear polymers, $R_g/R_h \approx 1.6$ and relatively constant, which is exactly the prediction from Zimm theory.⁵⁴ As the density of monomers increases, R_g/R_h is expected to decrease toward the hard sphere limit ($R_g/R_h = 0.77$).^{55,56} This is illustrated in the behavior of star polymers which show a decrease of $R_g/R_h = 1.4$ for a 3-armed polymer to $R_g/R_h = 1.08$ for a 270-arm polymer due to increasing concentration of monomers in the core of the molecule as the number of arms increases.⁵⁴ For our bottlebrush systems, we observe that at a fixed value of N_{bb} , as N_x decreases from 5 to 0, R_g/R_h decreases in response to the greater density of monomers. For $N_x = 0$, the densest of the bottlebrushes, we find that R_g/R_h decreases from approximately 1.2 at the smallest value of $R_{g,tot}$ to a minimum of $R_g/R_h \approx 1.1$ before increasing to $R_g/R_h \approx 1.3$ for the largest polymers. The eventual recovery of R_g/R_h as $R_{g,tot}$ (or equivalently, N_{tot}) increases is expected since random walk behavior is expected to emerge for sufficiently long backbones.²⁴ Our values of R_g/R_h are in reasonable agreement with those observed by Chremos and Douglas³¹ and Dutta et al.³⁷ The general trend of an initial decrease in R_g/R_h , followed by an increase as $R_{g,tot}$ increases persists for all values of N_x that we simulated. As we will demonstrate in the following sections, the

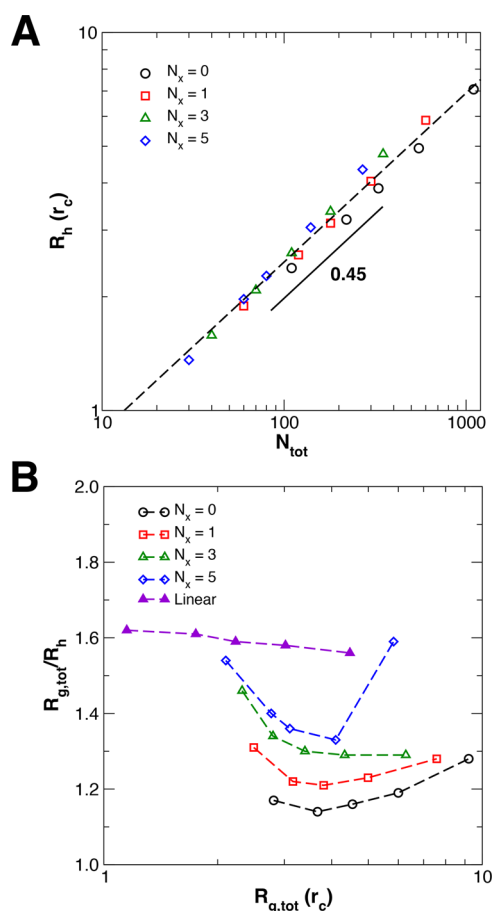


Figure 3. (A) Hydrodynamic radius (R_h) of the entire molecule as a function of its total degree of polymerization. Error bars are smaller than the points. (B) Ratio of $R_{g,tot}$ to R_h as a function of $R_{g,tot}$ (i.e., as molecular weight increases).

nonmonotonic behavior of R_g/R_h has implications for interpreting the relaxation dynamics of the bottlebrushes.

Modes of a Bottlebrush. As background, we briefly review some central properties of the Rouse model of polymer dynamics and compare the results of the model to numerical calculations for molecular bottlebrush relaxations. The Rouse model^{57,58} arises from solving the equations of motion for a series of N beads connected by $(N - 1)$ harmonic springs while neglecting hydrodynamic interactions. The equation of motion for each internal bead i is given by a Langevin equation

$$\frac{dr_i}{dt} = \frac{3k_B T}{b^2 \zeta} [r_{i+1} - 2r_i + r_{i-1}] + f_i \quad (7)$$

where ζ is the friction coefficient for the monomer and f_i is a Gaussian random force that is unique to monomer i . Analogous equations can be written for the beads at the ends of the chain.⁵⁸ Equation 7 can be cast into a convenient tridiagonal matrix form as

$$\frac{d}{dt} \begin{bmatrix} r_1 \\ r_2 \\ r_3 \\ \vdots \\ r_N \end{bmatrix} = \frac{3k_B T}{b^2 \zeta} \begin{bmatrix} -1 & 1 & 0 & 0 & \dots & 0 \\ 1 & -2 & 1 & 0 & \dots & 0 \\ 0 & 1 & -2 & 1 & \dots & 0 \\ \vdots & \ddots & \ddots & \ddots & \ddots & \vdots \\ 0 & 0 & 0 & \dots & 1 & -1 \end{bmatrix} \begin{bmatrix} r_1 \\ r_2 \\ r_3 \\ \vdots \\ r_N \end{bmatrix} + \begin{bmatrix} f_1 \\ f_2 \\ f_3 \\ \vdots \\ f_N \end{bmatrix} \quad (8)$$

or equivalently,

$$\frac{d}{dt} \mathbf{R} = \frac{3k_B T}{b^2 \zeta} \mathbf{A}_1 \mathbf{R} + \mathbf{F} \quad (9)$$

The large $N \times N$ matrix \mathbf{A}_1 in eqs 8 and 9 is a tridiagonal quasi-Toeplitz matrix, with corresponding cosine eigenvectors⁵⁹ that can be used to obtain the normal coordinates of the chain $X_p(t)$. The eigenvectors can be obtained by singular value decomposition (SVD). \mathbf{A}_1 represents the connectivity of a linear polymer and must be altered accordingly to describe bottlebrushes or other architectures. Each eigenvector of \mathbf{A}_1 captures the monomer displacement patterns of the chain for mode p .⁵⁰ As with POD, each eigenvector of \mathbf{A}_1 , when ordered by the decreasing magnitude of their corresponding eigenvalues, transforms the monomer coordinates to the normal coordinates according to eq 6. When ordered in this manner, each eigenvector corresponds to increasingly fast relaxation modes. As the magnitude of an eigenvalue decreases, the relaxation mode described by the corresponding eigenvector plays an increasingly small role. In fact, it is known that the amplitude of each mode quickly decreases as p increases.^{50,53}

Shown in Figure 4a is a comparison between the cosine functions in eq 3, derived analytically for the Rouse model (solid line),⁵⁸ along with the eigenvectors of \mathbf{A}_1 that were computed numerically from eq 9 for a linear polymer (circles) at a fixed degree of polymerization of $N = 30$ and for $p = 1$. The numerical results have been shifted by a constant phase of $\delta = \pi$ to match the analytical result, which does not affect the analysis of the dynamics.⁵⁰ The figure shows excellent quantitative agreement between the analytical theory and numerical calculation of the eigenvectors. We also compare these functions to the results of applying POD to DPD simulations of a linear homopolymer ($N = 30$) and the backbone of a bottlebrush ($N_{bb} = 30$, $N_{sc} = 10$, $N_x = 0$). As shown by the square (linear chain) and diamond (bottlebrush backbone) points in Figure 4a, there is excellent quantitative agreement among all three approaches. This suggests that Rouse mode analysis using the transformation in eq 3 is sufficient for analyzing the dynamics of the bottlebrush backbone alone. These results also suggest that the backbone of the bottlebrush in our simulations behaves as though it were simply a linear polymer, and the time scales of its motions are modulated by the presence of the grafted side chains as previously hypothesized from experimental measurements.^{40,42} As implicit side chain models are developed to simplify simulations of bottlebrushes,⁶⁰ this similarity between the relaxation modes of linear polymers and bottlebrushes will enable facile simulations of their dynamics.

However, as seen from Figure 4(b,e), eq 3 does not hold for analyzing the dynamics of the entire bottlebrush, and the eigenvectors become more complex than for the linear case. To understand the behavior of the entire bottlebrush, we first

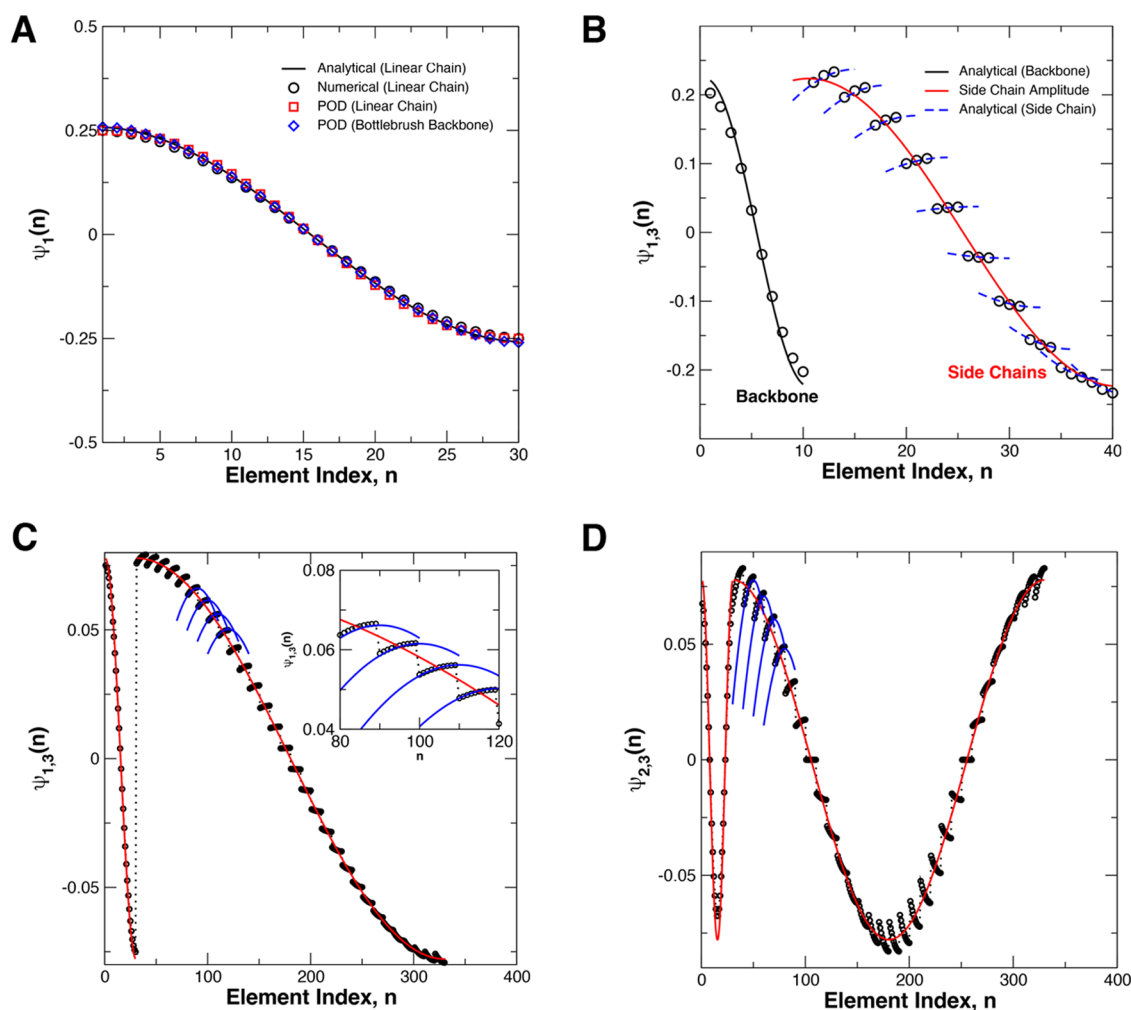


Figure 4. (A) Comparison of the analytical Rouse model (solid line) and eigenvectors obtained from numerical calculations (circles) for a linear chain. Eigenvectors from POD of DPD simulations for a linear chain (squares) and bottlebrush backbone (diamonds) show excellent quantitative agreement. (B) Eigenvector for the first mode of a bottlebrush ($N_{bb} = 10$, $N_{sc} = 3$, $N_x = 0$), calculated numerically along with analytical results overlaid as solid lines. The red line is the amplitude of the side chain portions, while the blue dashed lines describe the side chain motions. (C) Eigenvector of the first mode for a larger bottlebrush ($N_{bb} = 30$, $N_{sc} = 10$, and $N_x = 0$) calculated numerically. The inset shows a magnified view of the side chain region with the analytical results shown as blue lines. (D) Eigenvector of the $p = 2$ mode for the bottlebrush from panel (C), along with analytical results overlaid as solid lines.

numerically investigated a simple model molecule having $N_{bb} = 10$, $N_{sc} = 3$, and $N_x = 0$, resulting in a total degree of polymerization of $N_{tot} = 40$ with $n_s = 10$ side chains. The Rouse model for the bottlebrush can be cast into a form similar to that in eq 8 after small modifications to matrix A . With these modifications, A resembles a direct sum of A_1 and a series of similar matrices that describe each side chain along with off-diagonal elements that represent the bonding of the side chains to the backbone monomers. The resulting matrix (A_2) can be very large for realistic bottlebrushes with large molecular weights; for this simple example, A_2 is a 40×40 matrix and is shown in the Supporting Information (Equation S1). The eigenvector for $p = 1$ is plotted in Figure 4b as circular points. The elements of the eigenvector appear sinusoidal, and for elements $n > N_{bb}$, the function is piece-wise continuous. Discontinuities arise between sets of N_{sc} points for $n > N_{bb}$ as a result of boundary conditions imposed by grafting each side chain to the backbone.⁵³ For $n < N_{bb}$, the eigenvector is a cosine function identical to that obtained from the Rouse model: $\psi_1(n) = A_0 \cos[\pi/N_{bb}(n - 1/2)]$ (solid black line). For $n > N_{bb}$, each side chain produces small groupings of N_{sc} points

(n_s such groupings in all). This suggests that the first N_{bb} elements of the eigenvector describe the motion of the backbone, after which each set of N_{sc} points describes the motion of each side chain. Finally, we find that the side chain motions are also described by a cosine function but have a higher frequency of the backbone. For instance, if $p = 1$, we find that the side chain motions are described by $\cos[3\pi/(n_s N_{sc}(\dots))]$ (blue lines). Additionally, the amplitudes of the side chain functions vary as $\sqrt{2/N_{tot}} \cos[\pi/(n_s N_{sc})(n - N_{bb} - 1/2)]$ (solid red line), suggesting that the motions of the side chains are coupled to the backbone monomer to which they are attached.

Finally, we computed the eigenvectors using POD from DPD simulations to verify that the interpretation described above applied to our simulations. The comparison between the eigenvectors from the numerical approach to POD is shown in the Supporting Information, Figure S2. Although the two approaches produce very similar results, there are small numerical differences between the approaches that likely arise from the fact that POD is tracking the actual motions

of the monomers throughout the simulation, whereas the numerical approach represents an idealized molecule. We have observed similar differences in a previous study, and note that while the true Rouse modes obtained from SVD of A_2 arise from considering only the harmonic potential between bonded monomers, the modes produced by POD of the DPD simulations contain contributions from all of the forces that the monomers experience (i.e., from the conservative, random, and dissipative forces).⁴⁶

Although the analysis above was valid for $p = 1$, both the numerical solution and the POD approach provide the eigenvectors for higher-order modes. The next higher-order mode ($p = 2$) is plotted in Figure 4d. The eigenvector describing this mode is expected to be characterized by a backbone region with double the frequency of the $p = 1$ mode as well as a side chain region with an amplitude that varies in a similar fashion, all of which are present as indicated by the solid red lines. However, a full exploration of the behavior of all of the eigenvectors is beyond the scope of this article.

Bottlebrush Relaxation Dynamics. Representative autocorrelation functions $C_p(t)$ for $p = 1$ are presented in Figure 5a for (left to right) $N_{bb} = 10, 20, 30, 50,$ and 100 at constant

values of $N_{sc} = 10$ and $N_x = 1$. Open blue points correspond to calculations of $C_p(t)$ using only the backbone monomers, while solid black points correspond to $C_p(t)$ calculated using all of the monomers in the molecule. Red lines are fits to the exponential decay described in eq 4 using $\beta_p = 1$. For clarity, we show fits to only the $C_p(t)$ of the entire molecule. The relaxation times of the bottlebrush backbone and entire molecule are obtained by fitting their respective autocorrelation function.

For the shortest backbone ($N_{bb} = 10$), we find that the relaxation time of the backbone is faster than that of the entire molecule for all values of N_x , as shown by the faster decay of the blue points compared to the black points. However, as N_{bb} increases, the autocorrelation functions for the backbone and entire molecule become increasingly similar, and for $N_{bb} \geq 50$, they are almost indistinguishable. In Figure 5b, we plot the ratio of the relaxation time of the entire molecule (τ_1) to that of the backbone only ($\tau_{1,bb}$) as a function of N_{bb} for $N_x = 0-5$ at a fixed side chain length of $N_{sc} = 10$. The trend of the backbone relaxing faster than the entire molecule for smaller values of N_{bb} persists across all values of N_x that we considered, with the difference between the two relaxation times increasing as N_x increases. As N_{bb} decreases for a fixed number of side chains, the molecule increasingly resembles a star polymer. Since the relaxation time of the backbone decreases as N_{bb} decreases, the upward trend observed in Figure 5b is expected to persist and approach the total degree of polymerization of the polymer, i.e., $\tau_1/\tau_{1,bb} = \tau_0 N^\alpha / \tau_0 = N^\alpha$ as $N_{bb} \rightarrow 1$, where α is a scaling exponent. In contrast, for $N_{bb} \geq 50$, the difference between the two relaxation times becomes negligible, even for the largest side chain spacing of $N_x = 5$. This observation agrees well with the work of Ishaq et al.⁴¹ who measured the internal dynamics of ultralong bottlebrushes using DLS. By comparing the bottlebrush ($N_x \approx 1.5$) to ultralong linear polymers, they found that while the presence of side chains may result in longer relaxation times, ultimately the internal motions of the molecule were dictated by those of the backbone. Because $\tau_1/\tau_{1,bb} \rightarrow 1$ for sufficiently large values of N_{bb} , coarse-grained models with implicit side chains, such as those developed by Pan et al.,⁶⁰ are expected to correctly reproduce the dynamics of molecular bottlebrushes using the modes for linear polymers and Rouse mode analysis.

In Figure 6a, we plot τ_1 as a function of its radius of gyration for all of the systems that were simulated and compare the scaling of τ_1 for the bottlebrushes to linear polymers (filled triangles). The relaxation times for all bottlebrush polymers fall onto a single curve, indicating a similar scaling behavior for all polymers with that architecture, whereas the linear polymers follow a different scaling behavior. Despite the fact that the bottlebrushes are in a dilute solution, we observe a scaling $\tau_1 \sim R_g^{3.4}$, which is between the predictions of the Zimm ($\tau_1 \sim R_g^3$) and Rouse models ($\tau_1 \sim R_g^4$ for $\nu = 0.5$). This scaling appears to hold true even for $N_x = 5$, where the side chains are relatively far from each other. In contrast, for the linear polymers, $\tau_1 \sim R_g^{2.7}$, which is close to the Zimm prediction of $\tau_1 \sim R_g^3$. We showed previously using DPD and POD, with the same parameters as in this work, that the linear polymers exhibit a scaling $\tau_1 \sim N^{9/5}$, which is exactly the Zimm prediction for polymer coils with $\nu = 3/5$.⁴⁶ Thus, while linear chains follow a scaling law predicted by the Zimm model in dilute solutions, bottlebrushes follow a different scaling law with respect to their radius of gyration. Previous studies have observed differences between the scaling laws of the dynamics of linear polymers,

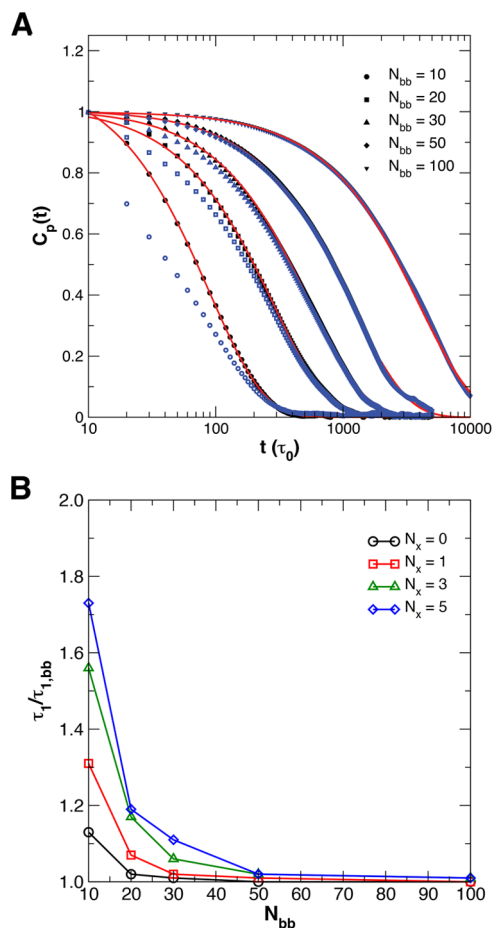


Figure 5. (A) Normal coordinate autocorrelation function $C_p(t)$ for $p = 1$ plotted as a function of time for different backbone lengths ($N_{sc} = 10$ and $N_x = 1$). Open blue points are from the backbone monomers only, while solid black points result from considering all monomers. Red lines are fits to an exponential decay. (B) Ratio of the longest relaxation time of the entire molecule (τ_1) to that of the backbone ($\tau_{1,bb}$) plotted as a function of backbone length for different values of N_x . Lines are guides for the eye.

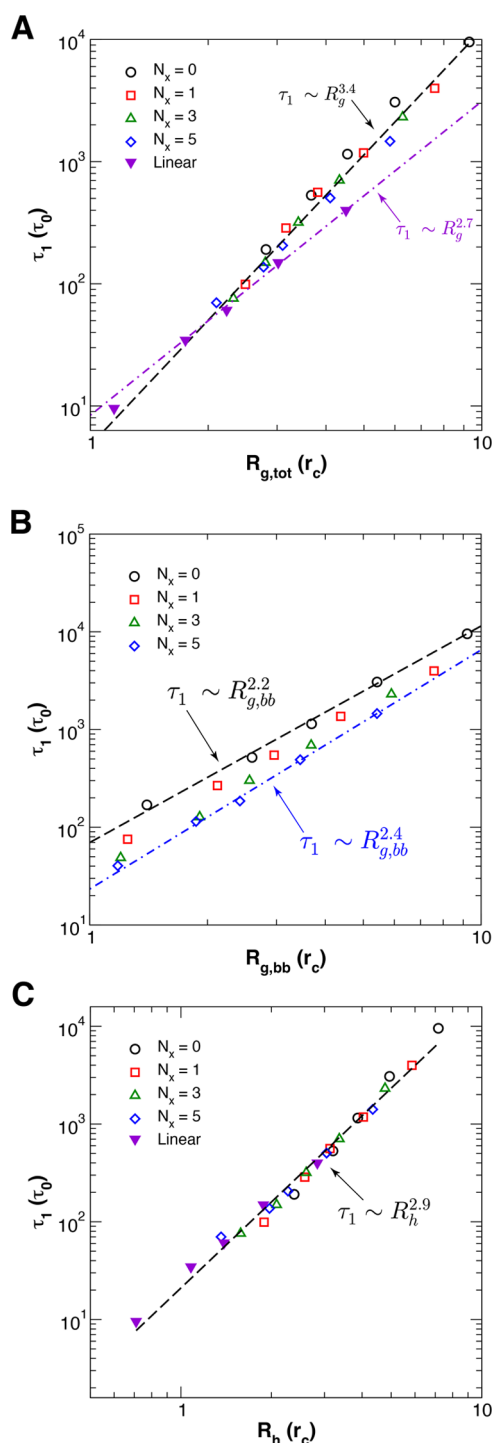


Figure 6. (A) Longest relaxation time of the entire bottlebrush (τ_1) plotted as a function of the radius of gyration of the molecule for all values of N_{bb} and N_x that were simulated. The dashed black line is a least-squares fit to the data, showing $\tau_1 \sim R_g^{3.4}$. (B) Longest relaxation time of the backbone ($\tau_{1, \text{bb}}$) plotted as a function of the backbone radius of gyration ($R_{g, \text{bb}}$) for different values of N_x . (C) τ_1 plotted as a function of R_h , showing quantitative agreement with the predictions of the Zimm model. For all data, error bars are smaller than the size of the points.

linear polymers under cylindrical confinement, and star polymers in dilute solutions.^{46,61} As shown in Figure 3b, R_g/R_h varies with bottlebrush molecular weight, indicating that the scaling law observed in Figure 6a may be influenced by R_g and

R_h scaling differently with molecular weight for different architectures. In particular, while the linear chains display a constant $R_g/R_h \approx 1.6$, the bottlebrushes show a decrease in this ratio to a minimum value, followed by a subsequent increase as molecular weight increases.

These computational results can be compared to recent experimental neutron spin-echo (NSE) measurements taken by Bichler et al.,⁴⁵ where the behaviors of two PDMS-g-PDMS bottlebrushes were compared. In one sample, the side chain length was relatively short, and NSE measurements were sensitive to the relaxations of the backbone. The second sample had an identical backbone length but long side chains such that NSE measurements observed relaxations similar to the “entire molecule” relaxations that are presented in our current work. For the sample with long side chains, a scaling $\tau_1 \sim Q^{-3.9}$ was observed, where Q is the scattering vector, implying that $\tau_1 \sim R_{g, \text{tot}}^{3.9}$. This result is very close to our results in Figure 6a. In contrast, for the short side chain sample, $\tau_1 \sim Q^{-2.5}$, implying $\tau_1 \sim R_{g, \text{bb}}^{2.5}$. The relaxation time of the backbone ($\tau_{1, \text{bb}}$) is plotted as a function of $R_{g, \text{bb}}$ for our simulations in Figure 6b. Although there are slight variations in the scaling of $\tau_{1, \text{bb}}$ with $R_{g, \text{bb}}$ for different values of N_x , the scaling exponents are similar to each other and roughly between 2.2 and 2.4, implying that one might expect experimentally to observe a scaling close to $\tau_{1, \text{bb}} \sim Q^{-2.4}$, as Bichler et al. measured.⁴⁵ Our simulations support Bichler et al.’s hypothesis that NSE measurements of the lower-molecular-weight side chain sample are sensitive to the backbone relaxations, while measurements of the higher-molecular-weight side chain sample probe relaxations more akin to the “entire molecule” relaxation times presented here. In addition, our results indicate that although the relaxation times of the backbone and entire molecule may be similar to one another (Figure 5b) for large values of N_{bb} , their scaling with length or scattering vector are different. To further explore this point, future neutron scattering measurements taking advantage of deuterated monomers and contrast matching would be well-warranted, in terms of both better understanding the relaxation dynamics and scaling of the backbone/bottlebrush radius of gyration.

To account for the nonmonotonic behavior of R_g/R_h with increasing molecular weight, we investigated the scaling of τ_1 as a function of R_h (Figure 6c) where we observe that for all values of chain length, side chain spacing, and architecture (linear versus bottlebrush), the relaxation times collapse onto a single curve. The scaling of the longest relaxation time is $\tau_1 \sim R_h^{2.9}$ which is in agreement with the prediction of Zimm for polymers in dilute solutions. Dutta et al. examined the scaling of the intrinsic viscosity of bottlebrush solutions with N_{bb} , and they found intrinsic viscosity scaled as predicted by the Zimm model. In analyzing their NSE measurements, Bichler et al. calculated an intrinsic relaxation time ($\langle \tau \rangle_{\text{int}}$) that accounted for the local structure of the solution and found that it scaled as $\langle \tau \rangle_{\text{int}} \sim Q^{-2.8}$. Not only is this prediction in quantitative agreement with the Zimm description of polymer dynamics but it is also in quantitative agreement with our results here.

CONCLUSIONS

In summary, we performed numerical analysis and dissipative particle dynamics (DPD) simulations of dilute solutions of molecular bottlebrushes. Proper orthogonal decomposition (POD) was used to extract the modes of the bottlebrushes so that mode analysis could be performed to observe the behavior of their relaxation times. Representative snapshots from the

simulations as well as quantitative analysis of the radius of gyration of the bottlebrush indicated that our DPD simulations reproduce the expected conformation of a bottlebrush in dilute solutions.

The relaxation modes obtained from POD were found to be in good agreement with those computed by numerically solving the Rouse model for small model systems. The backbone displays the same modes as a linear chain, while the entire bottlebrush showed more complicated modes that accounted for monomer displacements along the backbone that were coupled to the relaxations of the side chains. Some interpretation was provided for the first few modes. Mode analysis successfully produced relaxation times which matched neutron scattering experiments in terms of the scaling of τ_1 with a backbone radius of gyration.

Finally, we noted that although our DPD simulations confirmed that linear polymers had relaxation times that scaled according to the Zimm model, the relaxation times of the bottlebrush appeared to follow a different scaling law. The origin of this disagreement resides in the significant changes in bottlebrush shape that occur as N_{bb} increases, resulting in a ratio R_g/R_h that is not constant. When this behavior is accounted for, the dynamics of dilute bottlebrush solutions is well-described by Zimm dynamics. Future neutron scattering measurements that take advantage of deuterated monomers and contrast matching may provide further insight into the bottlebrush structure and dynamics by separately isolating scattering from the backbone and side chains relative to the entire molecule.

■ ASSOCIATED CONTENT

SI Supporting Information

The Supporting Information is available free of charge at <https://pubs.acs.org/doi/10.1021/acs.macromol.3c02259>.

Matrix description of a bottlebrush; methods for calculating the hydrodynamic radius; and a comparison between the numerical and POD approaches for obtaining the relaxation modes (PDF)

■ AUTHOR INFORMATION

Corresponding Author

Michael J. A. Hore – Department of Macromolecular Science and Engineering, Case Western Reserve University, Cleveland, Ohio 44122, United States; orcid.org/0000-0003-2571-2111; Phone: +1 (216) 368-0793; Email: hore@case.edu

Author

Raj S. Mukkamala – Department of Macromolecular Science and Engineering, Case Western Reserve University, Cleveland, Ohio 44122, United States

Complete contact information is available at: <https://pubs.acs.org/10.1021/acs.macromol.3c02259>

Notes

The authors declare no competing financial interest.

■ ACKNOWLEDGMENTS

The authors thank the NSF PIRE Bioinspired Materials and Systems program (OISE-1844463) for supporting this work. This work made use of the High Performance Computing Resource in the Core Facility for Advanced Research Computing at Case Western Reserve University.

■ REFERENCES

- (1) Li, Z.; Tang, M.; Liang, S.; Zhang, M.; Biesold, G. M.; He, Y.; Hao, S.-M.; Choi, W.; Liu, Y.; Peng, J.; Lin, Z. Bottlebrush polymers: From controlled synthesis, self-assembly, properties to applications. *Prog. Polym. Sci.* **2021**, *116*, No. 101387.
- (2) Jha, S.; Dutta, S.; Bowden, N. B. Synthesis of ultralarge molecular weight bottlebrush polymers using Grubbs' catalysts. *Macromolecules* **2004**, *37*, 4365–4374.
- (3) Kawamoto, K.; Zhong, M.; Gadelrab, K. R.; Cheng, L.-C.; Ross, C. A.; Alexander-Katz, A.; Johnson, J. A. Graft-through synthesis and assembly of janus bottlebrush polymers from A-branch-B diblock macromonomers. *J. Am. Chem. Soc.* **2016**, *138*, 11501–11504.
- (4) Ogbonna, N. D.; Dearman, M.; Cho, C.-T.; Bharti, B.; Peters, A. J.; Lawrence, J. Topologically Precise and Discrete Bottlebrush Polymers: Synthesis, Characterization, and Structure-Property Relationships. *JACS Au* **2022**, *2*, 898–905.
- (5) Jakobi, B.; Bichler, K. J.; Sokolova, A.; Schneider, G. J. Dynamics of PDMS-g-PDMS Bottlebrush Polymers by Broadband Dielectric Spectroscopy. *Macromolecules* **2020**, *53*, 8450–8458.
- (6) Terao, K.; Takeo, Y.; Tazaki, M.; Nakamura, Y.; Norisuye, T. Polymacromonomer consisting of polystyrene. Light scattering characterization in cyclohexane. *Polym. J.* **1999**, *31*, 193–198.
- (7) Terao, K.; Nakamura, Y.; Norisuye, T. Solution properties of polymacromonomers consisting of polystyrene. 2. Chain dimensions and stiffness in cyclohexane and toluene. *Macromolecules* **1999**, *32*, 711–716.
- (8) Terao, K.; Hokajo, T.; Nakamura, Y.; Norisuye, T. Solution properties of polymacromonomers consisting of polystyrene. 3. Viscosity behavior in cyclohexane and toluene. *Macromolecules* **1999**, *32*, 3690–3694.
- (9) Terao, K.; Hayashi, S.; Nakamura, Y.; Norisuye, T. Solution properties of polymacromonomers consisting of polystyrene: 4. Translational diffusion coefficient in cyclohexane at the Θ temperature. *Polym. Bull.* **2000**, *44*, 309–316.
- (10) Kikuchi, M.; Mihara, T.; Jinbo, Y.; Izumi, Y.; Nagai, K.; Kawaguchi, S. Characterization of rodlike poly (n-hexyl isocyanate) macromonomers and their polymacromonomers by light scattering, SAXS, intrinsic viscosity, and scanning force microscopy. *Polym. J.* **2007**, *39*, 330–341.
- (11) Inoue, K.; Yamamoto, S.; Nakamura, Y. Dilute solution properties of a polymacromonomer consisting of a polystyrene main chain with polyisoprene side chains. Relation of molecular parameters to polymer segment interactions. *Macromolecules* **2013**, *46*, 8664–8670.
- (12) Pan, T.; Dutta, S.; Kamble, Y.; Patel, B. B.; Wade, M. A.; Rogers, S. A.; Diao, Y.; Guirionnet, D.; Sing, C. E. Materials Design of Highly Branched Bottlebrush Polymers at the Intersection of Modeling, Synthesis, Processing, and Characterization. *Chem. Mater.* **2022**, *34*, 1990–2024.
- (13) Cai, L.-H.; Kodger, T. E.; Guerra, R. E.; Pegoraro, A. F.; Rubinstein, M.; Weitz, D. A. Soft Poly (dimethylsiloxane) Elastomers from Architecture-Driven Entanglement Free Design. *Adv. Mater.* **2015**, *27*, 5132–5140.
- (14) Yablon, L. M.; Sanders, S. N.; Li, H.; Parenti, K. R.; Kumarasamy, E.; Fallon, K. J.; Hore, M. J. A.; Cacciuto, A.; Sfeir, M. Y.; Campos, L. M. Persistent multiexcitons from polymers with pendent pentacenes. *J. Am. Chem. Soc.* **2019**, *141*, 9564–9569.
- (15) Kang, N.; Cho, S.; Leonhardt, E. E.; Liu, C.; Verkhotoirov, S. V.; Woodward, W. H. H.; Eller, M. J.; Yuan, T.; Fitzgibbons, T. C.; Borguet, Y. P.; et al. Topological Design of Highly Anisotropic Aligned Hole Transporting Molecular Bottlebrushes for Solution-Processed OLEDs. *J. Am. Chem. Soc.* **2022**, *144*, 8084–8095, DOI: [10.1021/jacs.2c00420](https://doi.org/10.1021/jacs.2c00420).
- (16) Kruger, A. G.; Brucks, S. D.; Yan, T.; Cárcamo-Oyarce, G.; Wei, Y.; Wen, D. H.; Carvalho, D. R.; Hore, M. J. A.; Ribbeck, K.; Schrock, R. R.; Kiessling, L. L. Stereochemical control yields mucin mimetic polymers. *ACS Cent. Sci.* **2021**, *7*, 624–630.
- (17) Lee, P. W.; Isarov, S. A.; Wallat, J. D.; Molugu, S. K.; Shukla, S.; Sun, J. E.; Zhang, J.; Zheng, Y.; Lucius Dougherty, M.; Konkolewicz,

- D.; et al. Polymer structure and conformation alter the antigenicity of virus-like particle-polymer conjugates. *J. Am. Chem. Soc.* **2017**, *139*, 3312–3315.
- (18) Nguyen, H. V.-T.; Jiang, Y.; Mohapatra, S.; Wang, W.; Barnes, J. C.; Oldenhuis, N. J.; Chen, K. K.; Axelrod, S.; Huang, Z.; Chen, Q.; et al. Bottlebrush polymers with flexible enantiomeric side chains display differential biological properties. *Nat. Chem.* **2022**, *14*, 85–93.
- (19) Verduzco, R.; Li, X.; Pesek, S. L.; Stein, G. E. Structure, function, self-assembly, and applications of bottlebrush copolymers. *Chem. Soc. Rev.* **2015**, *44*, 2405–2420.
- (20) Trefonas, P., III; Thackeray, J. W.; Sun, G.; Cho, S.; Clark, C.; Verkhoturov, S. V.; Eller, M. J.; Li, A.; Pavia-Sanders, A.; Schweikert, E. A.; et al. Bottom-up/top-down, high-resolution, high-throughput lithography using vertically assembled block bottle brush polymers. *J. Micro/Nanolithogr., MEMS, MOEMS* **2013**, *12*, No. 043006, DOI: 10.1117/1.JMM.12.4.043006.
- (21) Liberman-Martin, A. L.; Chu, C. K.; Grubbs, R. H. Application of bottlebrush block copolymers as photonic crystals. *Macromol. Rapid Commun.* **2017**, *38*, No. 1700058.
- (22) Arrington, K. J.; Radzinski, S. C.; Drummey, K. J.; Long, T. E.; Matson, J. B. Reversibly cross-linkable bottlebrush polymers as pressure-sensitive adhesives. *ACS Appl. Mater. Interfaces* **2018**, *10*, 26662–26668.
- (23) Yethiraj, A. A Monte Carlo simulation study of branched polymers. *J. Chem. Phys.* **2006**, *125*, No. 204901.
- (24) Hsu, H.-P.; Paul, W.; Rathgeber, S.; Binder, K. Characteristic length scales and radial monomer density profiles of molecular bottlebrushes: Simulation and experiment. *Macromolecules* **2010**, *43*, 1592–1601.
- (25) Birshtein, T.; Borisov, O.; Zhulina, Y.; Khokhlov, A.; Yurasova, T. Conformations of comb-like macromolecules. *Polym. Sci. USSR* **1987**, *29*, 1293–1300.
- (26) Gadelrab, K. R.; Alexander-Katz, A. Effect of molecular architecture on the self-assembly of bottlebrush copolymers. *J. Phys. Chem. B* **2020**, *124*, 11519–11529.
- (27) Rathgeber, S.; Pakula, T.; Wilk, A.; Matyjaszewski, K.; Lee, H. I.; Beers, K. L. Bottle-brush macromolecules in solution: Comparison between results obtained from scattering experiments and computer simulations. *Polymer* **2006**, *47*, 7318–7327, DOI: 10.1016/j.polymer.2006.06.010.
- (28) Theodorakis, P. E.; Hsu, H.-P.; Paul, W.; Binder, K. Computer simulation of bottle-brush polymers with flexible backbone: Good solvent versus theta solvent conditions. *J. Chem. Phys.* **2011**, *135*, No. 164903.
- (29) Liang, H.; Cao, Z.; Wang, Z.; Sheiko, S. S.; Dobrynin, A. V. Combs and Bottlebrushes in a Melt. *Macromolecules* **2017**, *50*, 3430–3437.
- (30) Lyubimov, I.; Wessels, M. G.; Jayaraman, A. Molecular dynamics simulation and PRISM theory study of assembly in solutions of amphiphilic bottlebrush block copolymers. *Macromolecules* **2018**, *51*, 7586–7599.
- (31) Chremos, A.; Douglas, J. F. A comparative study of thermodynamic, conformational, and structural properties of bottlebrush with star and ring polymer melts. *J. Chem. Phys.* **2018**, *149*, No. 044904.
- (32) Liang, H.; Wang, Z.; Sheiko, S. S.; Dobrynin, A. V. Comb and bottlebrush graft copolymers in a melt. *Macromolecules* **2019**, *52*, 3942–3950.
- (33) Wessels, M. G.; Jayaraman, A. Molecular dynamics simulation study of linear, bottlebrush, and star-like amphiphilic block polymer assembly in solution. *Soft Matter* **2019**, *15*, 3987–3998.
- (34) Wessels, M. G.; Jayaraman, A. Self-assembly of amphiphilic polymers of varying architectures near attractive surfaces. *Soft Matter* **2020**, *16*, 623–633.
- (35) Pesek, S. L.; Li, X.; Hammouda, B.; Hong, K.; Verduzco, R. Small-angle neutron scattering analysis of bottlebrush polymers prepared via grafting-through polymerization. *Macromolecules* **2013**, *46*, 6998–7005.
- (36) Pesek, S. L.; Xiang, Q.; Hammouda, B.; Verduzco, R. Small-angle neutron scattering analysis of bottlebrush backbone and side chain flexibility. *J. Polym. Sci., Part B: Polym. Phys.* **2017**, *55*, 104–111, DOI: 10.1002/polb.24251.
- (37) Dutta, S.; Wade, M. A.; Walsh, D. J.; Guironnet, D.; Rogers, S. A.; Sing, C. E. Dilute solution structure of bottlebrush polymers. *Soft Matter* **2019**, *15*, 2928–2941.
- (38) Sunday, D. F.; Chremos, A.; Martin, T. B.; Chang, A. B.; Burns, A. B.; Grubbs, R. H. Concentration Dependence of the Size and Symmetry of a Bottlebrush Polymer in a Good Solvent. *Macromolecules* **2020**, *53*, 7132–7140.
- (39) Sunday, D. F.; Martin, T. B.; Chang, A. B.; Burns, A. B.; Grubbs, R. H. Addressing the challenges of modeling the scattering from bottlebrush polymers in solution. *J. Polym. Sci.* **2020**, *58*, 988–996.
- (40) Dalsin, S. J.; Hillmyer, M. A.; Bates, F. S. Linear rheology of polyolefin-based bottlebrush polymers. *Macromolecules* **2015**, *48*, 4680–4691.
- (41) Ishaq, M. W.; Hao, N.; Zhu, M.; Li, L. Light scattering study of internal motions of ultralong comb-like chains in dilute solutions under good solvent conditions. *Macromolecules* **2020**, *53*, 558–568.
- (42) Horkay, F.; Chremos, A.; Douglas, J. F.; Jones, L.; Lou, R.; Xia, J.; Systematic, Y. Systematic investigation of synthetic polyelectrolyte bottlebrush solutions by neutron and dynamic light scattering, osmometry, and molecular dynamics simulation. *J. Chem. Phys.* **2020**, *152* (19), No. 194904, DOI: 10.1063/5.0007271.
- (43) Bichler, K. J.; Jakobi, B.; Schneider, G. J. Dynamical Comparison of Different Polymer Architectures Bottlebrush vs Linear Polymer. *Macromolecules* **2021**, *54*, 1829–1837.
- (44) Bichler, K. J.; Jakobi, B.; Sakai, V. G.; Klapproth, A.; Mole, R. A.; Schneider, G. J. Short-Time Dynamics of PDMS-g-PDMS Bottlebrush Polymer Melts Investigated by Quasi-Elastic Neutron Scattering. *Macromolecules* **2020**, *53*, 9553–9562.
- (45) Bichler, K. J.; Jakobi, B.; Honecker, D.; Stingaciu, L. R.; Weldeghiorghis, T. K.; Collins, J. H.; Schneider, G. J. Dynamics of Bottlebrush Polymers in Solution by Neutron Spin Echo Spectroscopy. *Macromolecules* **2022**, *55*, 9810–9819.
- (46) Miller, C. A.; Hore, M. J. Simulation of the Coronal Dynamics of Polymer-Grafted Nanoparticles. *ACS Polym. Au* **2022**, *2*, 157–168, DOI: 10.1021/acspolymersau.1c00031.
- (47) Spenley, N. A. Scaling laws for polymers in dissipative particle dynamics. *Europhys. Lett.* **2000**, *49*, 534.
- (48) Jiang, W.; Huang, J.; Wang, Y.; Laradji, M. Hydrodynamic interaction in polymer solutions simulated with dissipative particle dynamics. *J. Chem. Phys.* **2007**, *126*, No. 044901.
- (49) Besold, G.; Vattulainen, I.; Karttunen, M.; Polson, J. M. Towards better integrators for dissipative particle dynamics simulations. *Phys. Rev. E* **2000**, *62*, No. R7611.
- (50) Strobl, G. R. *The Physics of Polymers: Concepts for Understanding Their Structures and Behavior*; Springer Science & Business Media, 2007.
- (51) Wong, C. P. J.; Choi, P. Analysis of Brownian dynamics and molecular dynamics data of unentangled polymer melts using proper orthogonal decomposition. *Macromol. Theory Simul.* **2019**, *28*, No. 1800072, DOI: 10.1002/mats.201800072.
- (52) Ashwin, S. S. The Random Rouse block copolymer: Spectral Distribution of Randomly Segmented Tridiagonal quasi-Toeplitz Matrices *arXiv preprint arXiv:2202.10249* 2022.
- (53) Zimm, B. H.; Kilb, R. W. Dynamics of branched polymer molecules in dilute solution. *J. Polym. Sci.* **1959**, *37*, 19–42.
- (54) Rubinstein, M.; Colby, R. H. *Polymer Physics*; Oxford university press: New York, 2003; Vol. 23.
- (55) Mansfield, M. L.; Douglas, J. F.; Garboczi, E. J. Intrinsic viscosity and the electrical polarizability of arbitrarily shaped objects. *Phys. Rev. E* **2001**, *64*, No. 061401.
- (56) Hubbard, J. B.; Douglas, J. F. Hydrodynamic friction of arbitrarily shaped Brownian particles. *Phys. Rev. E* **1993**, *47*, No. R2983.

(57) Rouse, P. E., Jr A theory of the linear viscoelastic properties of dilute solutions of coiling polymers. *J. Chem. Phys.* **1953**, *21*, 1272–1280.

(58) Doi, M.; Edwards, S. F. *The Theory of Polymer Dynamics*; Oxford University Press, 1988; Vol. 73.

(59) Kulkarni, D.; Schmidt, D.; Tsui, S.-K. Eigenvalues of tridiagonal pseudo-Toeplitz matrices. *Linear Algebra Appl.* **1999**, *297*, 63–80, DOI: [10.1016/S0024-3795\(99\)00114-7](https://doi.org/10.1016/S0024-3795(99)00114-7).

(60) Pan, T.; Dutta, S.; Sing, C. E. Interaction potential for coarse-grained models of bottlebrush polymers. *J. Chem. Phys.* **2022**, *156*, No. 014903.

(61) Arnold, A.; Bozorgui, B.; Frenkel, D.; Ha, B.-Y.; Jun, S. Unexpected relaxation dynamics of a self-avoiding polymer in cylindrical confinement. *J. Chem. Phys.* **2007**, *127*, No. 164903, DOI: [10.1063/1.2799513](https://doi.org/10.1063/1.2799513).